Deceleration of Propagation Velocity and Reverse Propagation of MSTID Just Before the Major Earthquakes: Geostationary Satellite Observation for the 2019 Yamagata Earthquake and the 2019 Tanegashima Earthquake

Yuta Tsusaka[1], **Ken Umeno**[2]

[1,2]Department of Applied Mathematics and Physics, Graduate School of Informatics, Kyoto University, Kyoto, Japan

Key Points:

- We detected MSTID propagation decelerations only near the epicenter shortly before the 2019 Yamagata earthquake.
- We detected the reverse propagation of MSTID propagation only near the epicenter shortly before the 2019 Tanegashima nearshore earthquake.
- We interpreted these phenomena from the unified physical framework.

Corresponding author: Yuta Tsusaka, `tsusaka.yuta.64c@st.kyoto-u.ac.jp`

Abstract
In this study, we analyze the propagation of medium-scale traveling ionospheric disturbances (MSTIDs) immediately before earthquakes of M6 or greater magnitude that occurred between 2019 and 2021. We apply Correlation analysis and band-pass filter to TEC data obtained from the geostationary satellite QZS-3, and the results are compared to confirm the consistency of the results. As a result of the observation, we found that the propagation speed of MSTIDs decreased around the epicenter about 1 hour before the 2019 Yamagata earthquake and we detected a reverse propagation of the small-scale TID about 1 hour before the 2019 Tanegashima earthquake. These results are similar to the deceleration of MSTID propagation observed just before the 2016 Kumamoto earthquake (Umeno et al., 2021), and we propose that this is a kind of pattern of ionospheric anomalies just before the earthquake.

1 Introduction

The ionosphere is a region that extends from about 60 km to more than 1000 km above the ground, where some atmospheric molecules are ionized and have a high density of free electrons. The motion of electrons in the ionosphere is influenced by various natural phenomena, such as geomagnetic storms (Shagimuratov et al., 2002), solar flares (Donnelly, 1976), volcanic eruptions (Igarashi et al., 1994), and earthquakes (Astafyeva et al., 2011). Medium-Scale Traveling Ionospheric Disturbances (MSTIDs) are another type of disturbances that frequently occurs in the ionosphere, having a period of about 15 to 60 minutes and a horizontal wavelength of several hundred kilometers. Their occurrence frequency and propagation direction depend significantly on the season and time (Tsugawa et al., 2007; Otsuka et al., 2013).

Ionospheric anomalies before large earthquakes have been studied using various observation methods. The timescale also varies from a few days (Hayakawa et al., 1997; Liu et al., 2001) to a few tens of minutes before the event. Among these, anomalies of Total Electron Content (TEC) in the ionosphere has been reported $\sim$ 1 hour before the large earthquakes (Heki, 2011; Iwata & Umeno, 2016, 2017; Goto et al., 2019; Umeno et al., 2021; Heki, 2021). Heki observed positive anomalies of GPS-TEC about 40 minutes before the 2011 Tohoku-Oki earthquake(Heki, 2011). Besides, Iwata and Umeno 2016, 2017 reported a local TEC anomalies about 1 hour before the 2011 Tohoku-oki and 2016 Kumamoto-oki earthquakes by applying correlation analysis to GPS-TEC (Iwata & Umeno, 2016, 2017). On the other hand, re-analysis and rebuttal of Iwata and Umeno 2016, 2017 by Ikuta (Ikuta et al., 2021). In response to Ikuta (2021), Umeno et al. 2021 pointed out that their analysis was based on statistical values, and that in fact the MSTID velocity decrease just before the Kumamoto earthquake was a dynamic anomaly, making their counterargument off the mark. However, these objections by Umeno et al. 2021 were based on GPS and were made for only 2016 Kumamoto earthquake.

In this study, we examine whether that analysis is correct in a more general sense by (1) applying it to several different earthquakes other than the 2016 Kumamoto earthquake (2) using geostationary satellites (3) comparing CRA with another commonly used analysis method (band-pass filter). Specifically, we investigate the relationship between propagation velocities of MSTIDs and seismic activity in Japan, focusing on relatively large-scale earthquakes occurring between 2019 and 2021. We utilize the geostationary satellite of Japan's Quasi-Zenith Satellite System (QZSS) called "Michibiki,". By using the geostationary satellite, we can achieve higher-precision analysis due to the extended duration of TEC observations at the same location.

2 Methods

2.1 Correlation Analysis (CRA)

Correlation analysis is a signal processing technique used in the field of telecommunications to enhance the Signal-to-Noise (S/N) Ratio by examining the correlation between signals (Iwata & Umeno, 2016). In Iwata and Umeno (2017), correlation analysis was applied to GPS-TEC data, and as a result, an increase in correlation values was reported shortly before the occurrence of the 2016 Kumamoto earthquake. Below, we present the algorithm for correlation analysis.

Step 1: Let t_{sample} and t_{test} denote the lengths of sample data and test data (TEC) for the central station (station 0) and its surrounding stations (the number of surrounding stations is M).

Step 2: At station $i(= 0, 1, ..., M)$, approximate the sample data by a polynomial equation.

Step 3: Compute the prediction error $X_{i,t}$ between the test data and the polynomial prediction data approximated in Step 2.

Step 4: Take the correlation of $X_{i,t}$ between the central station and the surrounding stations as

$$C(T) = \frac{1}{M \times N} \sum_{i=1}^{M} \sum_{j=0}^{N-1} X_{0,t+t_{sample}+j\Delta t} \cdot X_{i,t+t_{sample}+j\Delta t} \tag{1}$$

$$T = t + t_{sample} + t_{test}, \tag{2}$$

where $C(T)$ is the TEC anomaly of the central station 0 at T.

Figure 1 depicts the propagation deceleration of MSTIDs (Medium-Scale Traveling Ionospheric Disturbances) immediately before the Kumamoto earthquake, as reported in Umeno et al. 2021. It clearly illustrates the delayed arrival of waves presumed to be MSTIDs about 40 minutes $\sim$ 1 hour before the earthquake. The band-pass filter is applied to the polynomially detrended TEC to check the consistency of the CRA results and the differences between the two methods.

2.2 Band-pass filter

Band-pass filter is a technique used in various fields to pass signals in a specific frequency range and attenuate or block signals outside that range. TID can be observed as periodic perturbations of TEC (Pedatella et al., 2010). We apply it to detrended TEC data as a comparison to CRA in order to detect MSTID and its propagation.

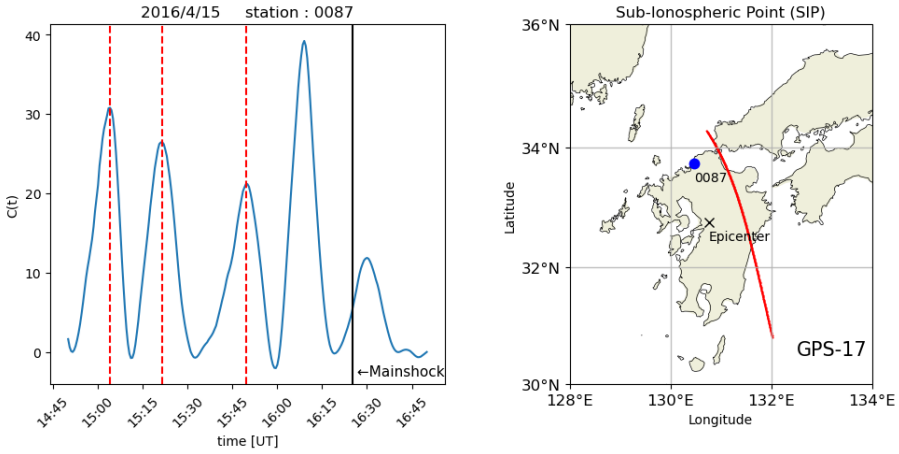

Figure 1. The MSTID propagation deceleration observed by correlation analysis about 40 minutes before the 2016 Kumamoto earthquake. The analysis utilizing GPS-17 with observation station 0087 as the central station are presented. The red lines in the left figure indicate the times, t_1, t_2, and t_3 ($t_1 < t_2 < t_3$), corresponding to the maxima of $C(t)$, where $\Delta T_1 \equiv t_2 - t_1 < \Delta T_2 \equiv t_3 - t_2$, clearly revealing the propagation deceleration.

3 Results

We focus on the direction and velocity of TID propagation immediately before the earthquake. Table 1 shows the presence or absence of TID around the time of the earthquake (M≥6) in Japan. Since the ionosphere is greatly affected by magnetic storms associated with solar activity and other factors, earthquakes that were accompanied by increased solar activity or magnetic storms around the time of the earthquake are excluded from the analysis. In fact, we exclude the September 13, 2021 earthquake on Off the Coast of Miyagi Prefecture from our analysis because solar activity was enhanced and the Dst and Kp indices indicate the occurrence of a magnetic storm at the time of the earthquake. We present below detailed results for the 2019 Yamagata and 2019 Tanegashima earthquakes, where significant anomalies were observed.

Table 1. Earthquakes with a magnitude of M6 or higher that have been analyzable using QZS-3 between 2019 and 2021.

Date [UT]	Epicentral location name	Magnitude	Depth	Presence of TID	Geomagnetic storm and solar activity
2019-01-08	Adjacent Sea of Tanegashima Island	6	30 km	Small-scale TID	quiet
2019-04-11	Off the Coast of Sanriku	6.2	5 km	×	quiet
2019-05-09	Hyuganada Sea	6.3	25 km	×(8h before)	quiet
2019-06-18	Off the Coast of Yamagata Prefecture	6.7	14 km	MSTID	quiet
2019-07-27	Off the southeast Coast of Mie Prefecture	6.6	393 km	×	quiet
2019-08-28	Off the east Coast of Aomori Prefecture	6.1	21 km	×	quiet
2020-04-19	Off the Coast of Miyagi Prefecture	6.2	46 km	×	quiet
2020-05-03	Off the west Coast of Satsuma Peninsula	6.2	9 km	×	quiet
2020-06-24	Off the east Coast of Chiba Prefecture	6.1	36 km	×(4h before)	quiet
2020-09-12	Off the Coast of Miyagi Prefecture	6.2	43 km	×	quiet
2020-12-20	Off the east Coast of Aomori Prefecture	6.5	43 km	×(12h before)	quiet
2021-03-20	Off the Coast of Miyagi Prefecture	6.9	59 km	×	active
2021-09-13	Off the south Coast of Tokaido	6	385 km	Small-scale TID	quiet
2021-12-09	Adjacent Sea of Tokara Islands	6.1	14 km	×	quiet

The 2019 Yamagata earthquake, which occurred on June 18, 2019, at 13:22 UT, was a relatively large earthquake with a magnitude of Mw 6.4 and a focal depth of 12 kilometers. Figure 2 (A) shows the spatial relationship between the epicenter of the 2019

Yamagata earthquake and the positions of key GNSS stations. Figure 2 (B) shows time series of C(t) obtained by applying correlation analysis to TEC near the epicenter just before the earthquake. From approximately 2 hours before the earthquake, MSTIDs were propagating in the southwest direction across Japan, and consistently propagating with a uniform periodicity until around 12:00 UT. Conversely, approximately 1 hour before the earthquake (around 12:20 UT), the peak of MSTIDs reaching the epicenter is delayed, as inferred by comparing it with MSTIDs that had already arrived. By estimating the deceleration time of MSTIDs from the C(t) of the 10 observation stations shown in Figure 2, the change in their velocity was determined to be $\Delta v = 30$ m/s.

Figure 3 (A) presents the temporal distribution of C(t) using approximately 1300 electron reference points across Japan, with distance in the southwest direction relative to a reference line on the vertical axis. MSTIDs were observable around the time of the earthquake occurrence. Moreover, the variations in MSTID velocity (changes in slope) are evident (as can be seen from Figure 3 (C)), and the estimated magnitude of this change is approximately 50 to 80 m/s. On the other hand, as shown in Figure 3 (B), the band-pass filter could not detect any obvious propagation deceleration of MSTID. This may be due to the inability to set the appropriate band to pass through the TID before and after deceleration.

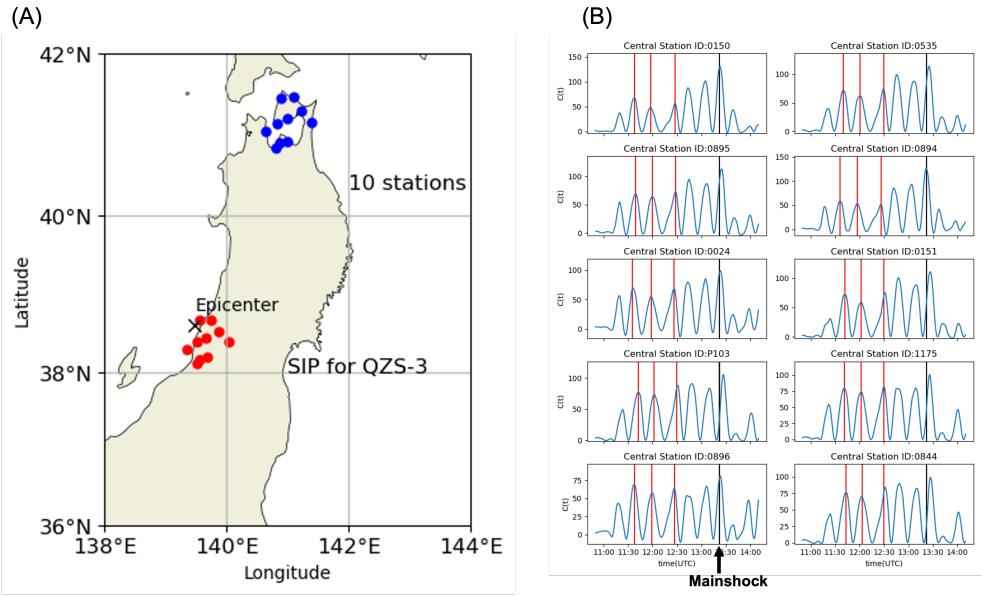

Figure 2. (A) The epicenter of the 2019 Yamagata earthquake (×), the positions of the 10 observation stations used for analysis (blue circles), and the Sub-Ionospheric Points (SIPs) relative to QZS-3 (red circles). (B) Temporal evolution of Total Electron Content (TEC) correlation values, denoted as C(t), at ten observation stations equipped with QZS-3 SIPs in the vicinity of the epicenter of the 2019 Yamagata earthquake. The black line represents the earthquake occurrence time. Red lines indicate the times, t_1, t_2, and t_3 ($t_1 < t_2 < t_3$), corresponding to the maxima of $C(t)$, where $\Delta T_1 \equiv t_2 - t_1 < \Delta T_2 \equiv t_3 - t_2$, clearly revealing the propagation deceleration.

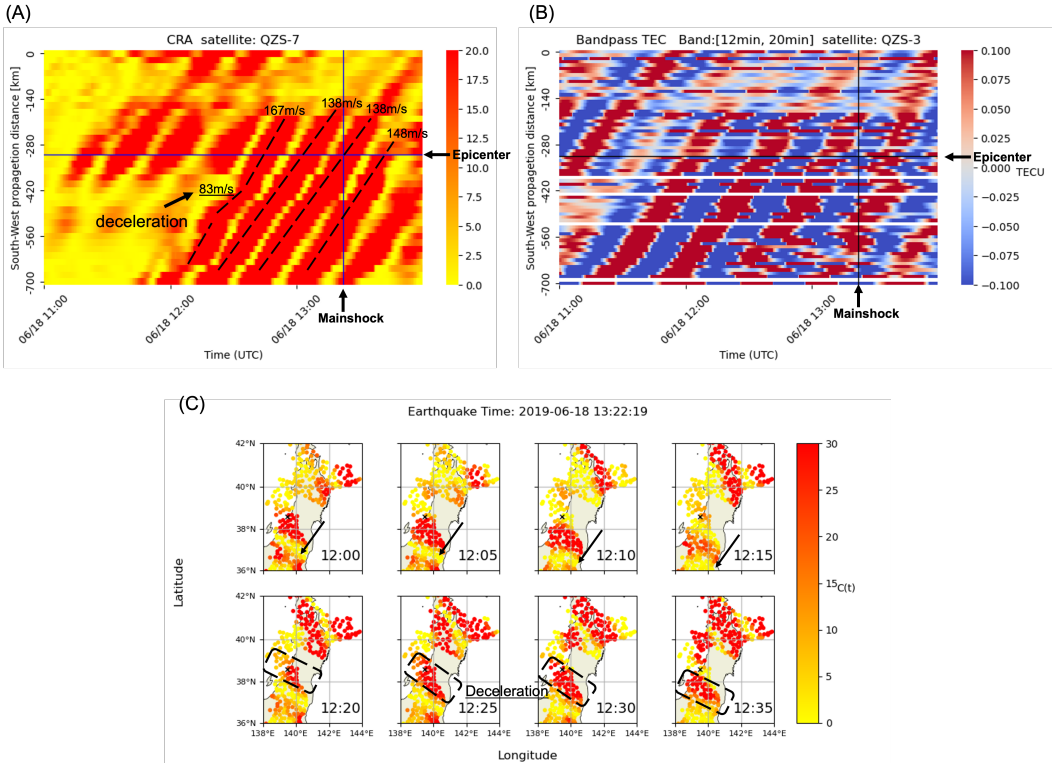

Figure 3. (A) A heatmap of TEC correlation values, C(t), just before the 2019 Yamagata earthquake. The vertical axis represents the distance between each observation station and the SIP relative to QZS-3, orthogonal to the direction of MSTID propagation. (B) A heatmap of filterd TEC with band [12min, 20min] just before the 2019 Yamagata earthquake. The vertical axis represents the distance between each observation station and the SIP relative to QZS-3, orthogonal to the direction of MSTID propagation. (C) Time evolution of TEC correlation C(t) near the epicenter just before the Yamagata earthquake

For the 2019 Tanegashima nearshore earthquake, MSTIDs did not occur just before the earthquake, but small-scale disturbances were propagating in the southwest direction. Figure 4 (A) is a heatmap of TEC correlation values, C(t), just before the 2019 Tanegashima earthquake. The small-scale TID propagating in the southwest direction was observed between 10:00UT and 11:00UT. After 11:30UT (approximately 1 hour before the earthquake), it started propagating in the northeast direction, indicating the reverse propagation. The change in propagation velocity of small-scale TID is estimated to be approximately 650-700 m/s. Figure 4 (B) similarly shows the results of the band-pass filter. Unlike the case of the 2019 Yamagata earthquake (Figure 4 (B)), it can be seen that the band-pass filter was also able to detect propagation anomalies (velocity changes). The reason for this may be that while the direction was reversed before and after the velocity change, the magnitudes of the velocities were relatively close, so there was a band that could detect the TID before and after the change. These results suggest that CRA is a more versatile method for detecting velocity changes of TID. This property will also be important in the implementation of real-time observations.

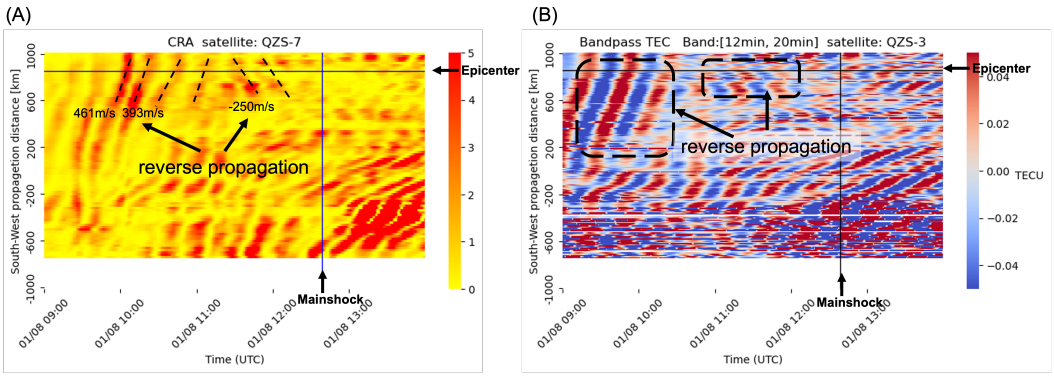

Figure 4. (A) A heatmap of TEC correlation values, C(t), just before the 2019 Tanegashima earthquake. The vertical axis represents the distance between each observation station and the QZS-3 SIP, orthogonal to the direction of MSTID propagation. (B) A heatmap of filterd TEC with band [12min, 20min] just before the 2019 Tanegashima earthquake. The vertical axis represents the distance between each observation station and the SIP relative to QZS-3, orthogonal to the direction TID propagation.

4 Discussion

In Umeno et al. 2021, the relationship between the north-south velocity change Δv (positive for northward motion) of MSTIDs and the variation in the east-west electric field ΔE (positive for eastward direction) in the ionosphere is derived from plasma equations as shown in Equation (3):

$$\frac{\Delta v}{\Delta E} = \frac{e}{m_i \Omega_i} \simeq 6 \times 10^4 \ \mathrm{T}^{-1} \tag{3}$$

Here, e represents the elementary charge, m_i is the ion mass, and Ω_i is the ion cyclotron angular frequency. Based on the results in Section 3, the deceleration of MSTIDs just before the 2019 Yamagata earthquake ranges from 30 to 80 m/s. From Equation (3), it can be inferred that ΔE varies from a minimum of 0.50 mV/m to a maximum of 1.33 mV/m in the eastward direction. In Umeno et al. 2021, the required electric field change for ionospheric anomalies (MSTID propagation deceleration) just before the 2016 Kumamoto earthquake was estimated to be approximately 0.58 mV/m, which is almost the same estimation by Kelley et al. 2017 and Heki 2021 for the variation in the ionospheric electric field required for ionospheric anomalies just before the 2011 Tohoku offshore earthquake to be 0.5 mV/m (Kelley et al., 2017; Heki, 2021). The estimated range of 0.50 to 1.33 mV/m in this study is consistent with these results.

Next, we discuss propagation deceleration and reverse by using the model presented in Equation (3). A type of MSTID propagation anomaly varies based on the magnitude relationship between the steady-state velocity of MSTID (v) and the velocity change (Δv). We infer that in the case of the Yamagata earthquake, $v > \Delta v$, which means that TID propagation deceleration occurred, while in the case of the Tanegashima earthquake, $v < \Delta v$, which means that propagation was reversed. Therefore, propagation deceleration and reverse propagation are two manifestations of the same phenomenon and can be explained using a unified physical model.

Finally, table 2 summarizes the presence of TID and its propagation anomalies immediately before the earthquakes to be analyzed. MSTIDs were observed only for the 2019 Yamagata earthquake that occurred on June 18, 2019 and the deceleration of MSTID propagation velocity were observed near the epicenter 1 hour before the earthquake. Similar results were obtained for the Off the south Coast of Tokaido earthquake in 2021, where the velocity of the small-scale TID had decreased before the earthquake. On the other hand, no MSTID propagation anomaly was observed for any of the earthquakes shown in Table 1 (the 2019 Hyuganada Sea, the 2020 Off the east Coast of Chiba Prefecture, the 2020 Off the east Coast of Aomori Prefecture), where MSTIDs had been observed until several hours before the earthquake. Taking into account that the earthquakes for which propagation anomalies have been observed in previous studies and in this study commonly found propagation anomalies about 1 hour before the earthquake, there would be a limited window of the occurrence of the preseismic anomalies of TID propagation.

Table 2. The MSTID propagation anomalies just before earthquakes with a magnitude of M6 or higher that have been analyzable using QZS-3 between 2019 and 2021.

Date [UT]	Epicentral location name	M	Depth	Presence of MSTID	Propagation anomaly	Δv	ΔE	Anomaly time
2019-01-08	Adjacent Sea of Tanegashima Island	6	30 km	Small-scale	Reverse propagation	650.0m/s	10.8mV/m	1h before
2019-06-18	Off the Coast of Yamagata Prefecture	6.7	14 km	○	Deceleration	30.0 m/s	0.50mV/m	1h before
2021-09-13	Off the south Coast of Tokaido	6	385 km	Small-scale	Deceleration	107.0 m/s	1.78mV/m	1h before

5 Conclusion

Before the present work, TID propagation velocity changes shortly before large earthquakes were only reported in the single event (the 2016 Kumamoto earthquake). Here we conclude that this dynamic anomaly observed in the single event is not just a type of anomaly pattern but a general anomaly to be applied to other earthquakes, supporting the validity of the rebuttal analysis by Umeno et al. 2021 towards the Ikuta et al. 2021 as follows. We detected TID propagation velocity changes on a common timescale of about 1 hour before the earthquake in several earthquakes of M6 or greater, including the 2019 Yamagata earthquake. Among all the earthquakes with M≥6 during 2019-2021 around Japan, which we analyzed with the geostationary satellite QZS-3 here, anomalies were necessarily observed in all the types of earthquakes for which TID occurred near the epicenter within 1 hour of occurrence. These results suggest that *dynamic* changes in TID propagation velocity are related to the earthquakes, caused by unknown preparation process of the earthquakes and could be the candidate of precursors of the earthquakes with M≥6 based on the causal physical mechanism discussed in the previous section as proposed by Umeno et al. 2021. Furthermore, we estimate the magnitude of the ionospheric electric field required to cause these ionospheric anomalies and find it consistent with the results from the 2016 Kumamoto earthquake. In these analyses, we compared CRA and band-pass filter results and found that CRA is a more versatile method for detecting TID velocity changes. Future work includes analysis of earthquakes worldwide, implementation of real-time observations, and elucidation of physical mechanisms.

6 Open Research

The datasets analyzed in this study is available in the Kyoto University Research Information repository: `https://doi.org/10.57723/286320`

Acknowledgments
GNSS data used in this study is available through the following organizations: GSI (`https://terras.gsi.go.jp`).

References

Astafyeva, E., Lognonné, P., & Rolland, L. (2011). First ionospheric images of the seismic fault slip on the example of the Tohoku-oki earthquake. *Geophysical Research Letters*, *38*(22). doi: 10.1029/2011GL049623

Donnelly, R. F. (1976). Empirical models of solar flare X ray and EUV emission for use in studying their E and F region effects. *Journal of Geophysical Research (1896-1977)*, *81*(25), 4745–4753. doi: 10.1029/JA081i025p04745

Goto, S.-i., Uchida, R., Igarashi, K., Chen, C.-H., Kao, M., & Umeno, K. (2019). Preseismic Ionospheric Anomalies Detected Before the 2016 Taiwan Earthquake. *Journal of Geophysical Research: Space Physics*, *124*(11), 9239–9252. doi: 10.1029/2019JA026640

Hayakawa, Molchanov, Ondoh, & Kawai. (1997, May). On the precursory signature of Kobe earthquake on VLF subionospheric signals. In *1997 Proceedings of International Symposium on Electromagnetic Compatibility* (pp. 72–75). doi: 10.1109/ELMAGC.1997.617080

Heki, K. (2011). Ionospheric electron enhancement preceding the 2011 Tohoku-Oki earthquake. *Geophysical Research Letters*, *38*(17). doi: 10.1029/2011GL047908

Heki, K. (2021). Ionospheric Disturbances Related to Earthquakes. In *Ionosphere Dynamics and Applications* (pp. 511–526). American Geophysical Union (AGU). doi: 10.1002/9781119815617.ch21

Igarashi, K., Kainuma, S., Nishimuta, I., Okamoto, S., Kuroiwa, H., Tanaka, T., & Ogawa, T. (1994, July). Ionospheric and atmospheric disturbances around Japan caused by the eruption of Mount Pinatubo on 15 June 1991. *Journal of Atmospheric and Terrestrial Physics*, *56*(9), 1227–1234. doi: 10.1016/0021-9169(94)90060-4

Ikuta, R., Oba, R., Kiguchi, D., & Hisada, T. (2021). Reanalysis of the Ionospheric Total Electron Content Anomalies Around the 2011 Tohoku-Oki and 2016 Kumamoto Earthquakes: Lack of a Clear Precursor of Large Earthquakes. *Journal of Geophysical Research: Space Physics*, *126*(9), e2021JA029376. doi: 10.1029/2021JA029376

Iwata, T., & Umeno, K. (2016). Correlation analysis for preseismic total electron content anomalies around the 2011 Tohoku-Oki earthquake. *Journal of Geophysical Research: Space Physics*, *121*(9), 8969–8984. doi: 10.1002/2016JA023036

Iwata, T., & Umeno, K. (2017). Preseismic ionospheric anomalies detected before the 2016 Kumamoto earthquake. *Journal of Geophysical Research: Space Physics*, *122*(3), 3602–3616. doi: 10.1002/2017JA023921

Kelley, M. C., Swartz, W. E., & Heki, K. (2017). Apparent ionospheric total electron content variations prior to major earthquakes due to electric fields created by tectonic stresses. *Journal of Geophysical Research: Space Physics*, *122*(6), 6689–6695. doi: 10.1002/2016JA023601

Liu, J. Y., Chen, Y. I., Chuo, Y. J., & Tsai, H. F. (2001). Variations of ionospheric total electron content during the Chi-Chi Earthquake. *Geophysical Research Letters*, *28*(7), 1383–1386. doi: 10.1029/2000GL012511

Otsuka, Y., Suzuki, K., Nakagawa, S., Nishioka, M., Shiokawa, K., & Tsugawa, T. (2013, February). GPS observations of medium-scale traveling ionospheric disturbances over Europe. *Annales Geophysicae*, *31*(2), 163–172. doi: 10.5194/angeo-31-163-2013

Pedatella, N. M., Lei, J., Thayer, J. P., & Forbes, J. M. (2010). Ionosphere response to recurrent geomagnetic activity: Local time dependency. *Journal of Geophysical Research: Space Physics*, *115*(A2). doi: 10.1029/2009JA014712

Shagimuratov, I. I., Baran, L., Wielgosz, P., & Yakimova, G. A. (2002, May). The structure of mid- and high-latitude ionosphere during September 1999 storm event obtained from GPS observations. *Annales Geophysicae*, *20*(5), 655–660. doi: 10.5194/angeo-20-655-2002

Tsugawa, T., Kotake, N., Otsuka, Y., & Saito, A. (2007, March). Medium-scale traveling ionospheric disturbances observed by GPS receiver network in Japan: A short review. *GPS Solutions*, *11*(2), 139–144. doi: 10.1007/s10291-006-0045-5

Umeno, K., Nakabayashi, R., Iwata, T., & Kao, M. (2021, November). Capability of TEC correlation Analysis and Deceleration at Propagation Velocities of Medium-Scale Traveling Ionospheric Disturbances: Preseismic Anomalies before the Large Earthquakes. *Open Journal of Earthquake Research*, *10*(4), 105–137. doi: 10.4236/ojer.2021.104008